LEGIBILITY NOTICE

A major purpose of the Technical Information Center is to provide the broadest dissemination possible of information contained in DOE's Research and Development Reports to business, industry, the academic community, and federal, state and local governments.

Although a small portion of this report is not reproducible, it is being made available to expedite the availability of information on the research discussed herein.

1

LA-UR 89-3791

DEC 04 1989

Los Alamos National Laboratory is operated by the University of California for the United States Department of Energy under contract W-7405-ENG-36

LA-UR--89-3791

DE90 003214

TITLE: EFFECTS OF PARAMETRIC VARIATIONS OF COMPLEX TARGETS ON DAMAGE FROM PROJECTILE IMPACT

AUTHOR(S): Robert W. Meier

SUBMITTED TO: 1989 Hypervelocity Impact Symposium, December 12-14, 1989, San Antonio, Texas

DISCLAIMER

This report was prepared as an account of work sponsored by an agency of the United States Government. Neither the United States Government nor any agency thereof, nor any of their employees, makes any warranty, express or implied, or assumes any legal liability or responsibility for the accuracy, completeness, or usefulness of any information, apparatus, product, or process disclosed, or represents that its use would not infringe privately owned rights. Reference herein to any specific commercial product, process, or service by trade name, trademark, manufacturer, or otherwise does not necessarily constitute or imply its endorsement, recommendation, or favoring by the United States Government or any agency thereof. The views and opinions of authors expressed herein do not necessarily state or reflect those of the United States Government or any agency thereof.

By acceptance of this article, the publisher recognizes that the U.S. Government retains a nonexclusive, royalty-free license to publish or reproduce the published form of this contribution, or to allow others to do so, for U.S. Government purposes. The Los Alamos National Laboratory requests that the publisher identify this article as work performed under the auspices of the U.S. Department of Energy.

Los Alamos National Laboratory
Los Alamos, New Mexico 87545

MASTER

DISTRIBUTION OF THIS DOCUMENT IS UNLIMITED

EFFECTS OF PARAMETRIC VARIATIONS OF COMPLEX TARGETS ON DAMAGE FROM PROJECTILE IMPACT

ROBERT W. MEIER

Technical Engineering Support Group, Los Alamos National Laboratory
P.O. Box 1663, Los Alamos, New Mexico 87545

ABSTRACT

The effects of a hypervelocity projectile striking complex targets have been investigated. The targets consisted of metallic and low-density shock attenuating layers and void regions. The major features of the targets were systematically varied to correlate changes in the targets with the projectile's effectiveness in damaging the targets. Two-dimensional numerical simulations were done with the Eulerian computational fluid dynamics program PINON. Projectile effectiveness against the various targets was measured by determining the maximum pressure, pressure integral, $P^2\tau$ value, and hole size at several locations in the targets.

INTRODUCTION

Projectile interactions with complex targets are of interest in many different fields. The effects of various components of a target in influencing the behavior of an impacting projectile are not fully understood. The penetration of a projectile into a complex target is influenced by each of the material layers and void regions it encounters. Numerical simulation has been used to increase the understanding of projectile and target interactions (Johnson and Anderson 1987) and to investigate the effects of various projectiles on a complex target (Meier 1987). In this study the effects of a projectile striking different complex targets at a fixed velocity were investigated. To correlate the changes in the targets with the projectile's effectiveness in damaging the targets, several major features of complex targets were systematically varied.

The targets consisted of layers of silica phenolic and aluminum behind which was a void region. Behind the void region was a multilayered region of polyurethane foam (1.26 g/cm^3) between two layers of aluminum. The target structures and the projectile that struck them are shown in Fig. 1. In this figure the projectile motion is from left to right. The projectile was a tungsten sphere with a mass of 10 g. It struck the silica phenolic layer at 1 cm/μs. The projectile material, mass, and velocity were chosen to produce significant target damage across the spectrum of targets used in the study. The projectile impact conditions were held constant so that the effects of target parameters could be isolated.

The thicknesses of two of the aluminum layers shown in Fig. 1 were held constant, while the thicknesses of the silica phenolic, adjoining aleminum, and polyurethane foam layers and the extent of the void region were systematically varied. By systematically varying individual target characteristics while holding constant the other target parameters and the projectile impact conditions, it was possible to determine the projectile's effectiveness in penetrating and damaging the target with each variation in the target. Conversely, this procedure permitted determination of the effectiveness of each of the target characteristics in minimizing the damage and penetration caused by the projectile.

The variation range and the intermediate or nominal values of the target characteristics are shown in Table 1. The nominal value of each target characteristic was used, except for the layer that was being varied for that particular case. Each target characteristic was varied from its minimum to its maximum value and compared with the results achieved for its nominal value.

METHODOLOGY

The impact dynamics were simulated with the PINON computational fluid dynamics program. PINON is a state of the art program that uses Eulerian finite difference algorithms with a high order advection scheme. It also employs a unique interface reconstruction technique [illegible]

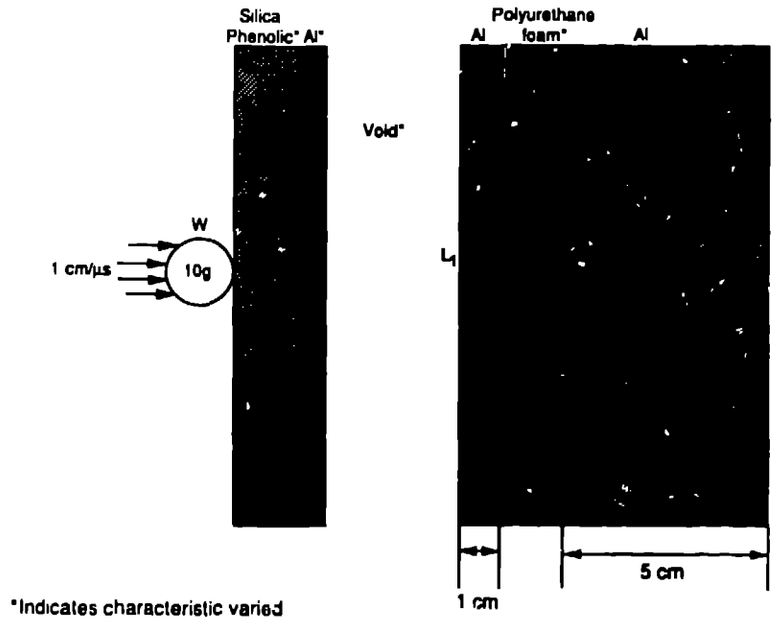

Fig. 1. Structure of targets simulated.

Table 1. Variation range of target characteristics

Layer	Minimum (cm)	Nominal (cm)	Maximum (cm)
Silica phenolic	1.0	2.5	3.0
Aluminum	0.2	1.0	2.0
Void	1.0	10.0	18.0
Polyurethane Foam	0.0	2.5	5.0

includes material strength (Youngs 1982). The only material strength included in the computations in this study was a simple strength model provided by negative pressures in the equations of state.

The targets consisted of a series of discs 30 cm in diameter and of one void region. The diameter was large enough to eliminate edge effects and to allow sufficient distance for the debris clouds to expand in the transverse direction. The computations were done in two-dimensional cylindrical geometry because there was no variation in the angular direction.

SESAME (Holian 1984, Boettger 1989) equations of state were used for all materials. The SESAME equation-of-state library is a standard, computer-based library that contains tables of thermodynamic properties for a wide range of materials over a wide range of physical regions SESAME is one of the most accurate collections of equations of state available.

The following SESAME equation-of-state numbers were used: No. 3542 for the tungsten projectile, No. 7580 for the silica phenolic layer, No. 3717 for the aluminum layers, and No. 7561 for the polyurethane foam layer. The equations-of-state for tungsten and aluminum are nonequilibrium types, while those for silica phenolic and polyurethane foam are equilibrium equations of state.

An investigation of the effect of finite difference cell size on solution accuracy showed that significant numerical errors were present in the solution when a 0.2 cm node spacing was used When a 0.05 cm node spacing was used, the computing time became excessive

Uniform node spacing of 0.1 cm was used to compute all results quoted in this paper. This computational cell size provided at least 10 cells across the width of all of the target layers except the aluminum layer that adjoins the silica phenolic layer at its minimum thickness. Because the projectile diameter was 1 cm, there were 10 computational cells across its diameter. Each target impact simulation typically required several hours of computing time on a Cray X-MP

so this node spacing was near the practical limit of fineness and produced good accuracy in computed pressures and target deformation.

Projectile effectiveness against the various targets was measured by calculating the instantaneous pressures, the time integrated pressure, and the $P^2\tau$ value along the centerline at the fronts of each of the aluminum layers (referred to as Location 1 and Location 2) in Section 2.* These values were measured on the projectile's line-of-travel (centerline of the axisymmetric geometry) because the greatest pressures were produced along this line. The pressure integrals and $P^2\tau$ values were calculated from the instantaneous pressure plots as functions of time. The integral of the pressure over time is a measure of the impulse per unit area. The $P^2\tau$ values were defined as the maximum pressures squared times the pulse widths at half the maximum pressure.

The $P^2\tau$ value is one criterion used to determine the threshold of shock initiation of explosives. The $P^2\tau$ criterion (Walker 1976) is based on the critical energy criterion (Walker & Wasley, 1969). A sufficiently high pressure is required for a sufficiently long period of time to achieve detonation. The $P^2\tau$ value combines both of these characteristics into a quantifiable measure. Target damage was also assessed by measuring the size of the hole produced in the silica phenolic and aluminum layers in front of the void region.

RESULTS

Target with Nominal Thickness Layers

Figure 2 shows a graphic of the target, with all the layers at their nominal thicknesses, 100 μs after being struck by the projectile. This density-weighted plot of the target primarily shows the deformation of the target layers, but it also shows some of the shock waves in the target. After 100 μs the target was still deforming, but the hole growth rate in Section 1 was very small. Therefore, the state of Section 1 of the target after 100 μs was a good approximation of the final damage caused by the projectile impact. In this case the projectile produced a hole in Section 1 that was 12 cm in diameter.

Typical pressures calculated at Locations 1 and 2 are shown in Figs. 3 and 4, respectively. Typically the pressure at Location 1 was much higher and more volatile than that at Location 2. This behavior was caused by the debris produced in the void region and the attenuating material between the two locations.

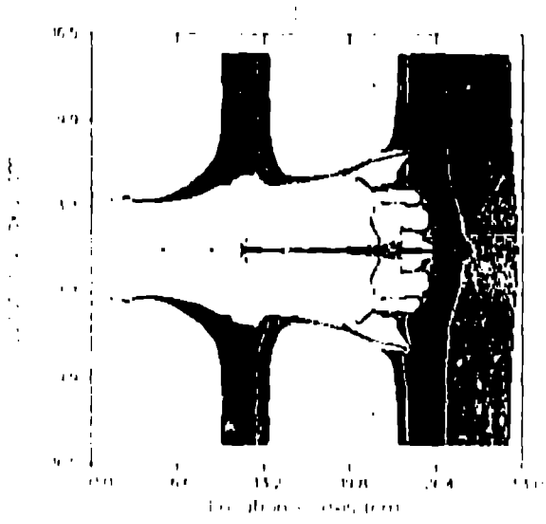

Fig. 2. Deformation of the nominal target.

* For convenience, the front target section of silica phenolic and aluminum will be referred to as Section 1 and the back section of the two aluminum layers separated by polyurethane foam will be referred to as Section 2.

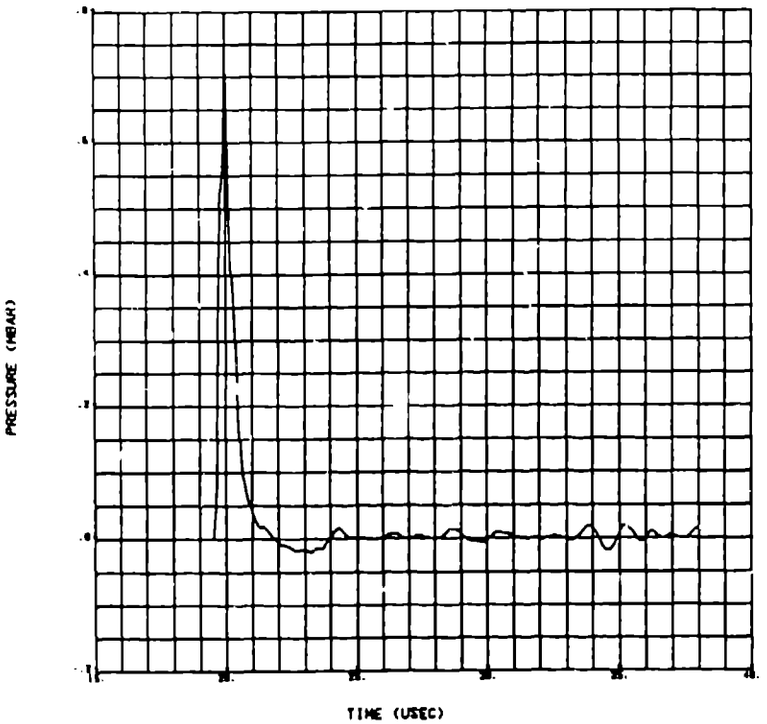

Fig. 3. Location 1 pressure in the nominal target.

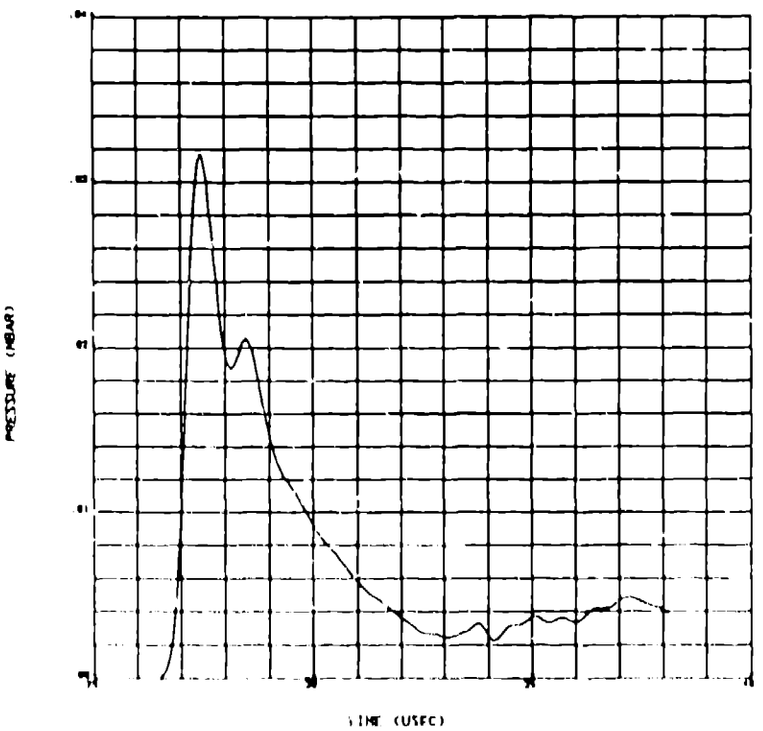

Fig. 4. Location 2 pressure in the nominal target.

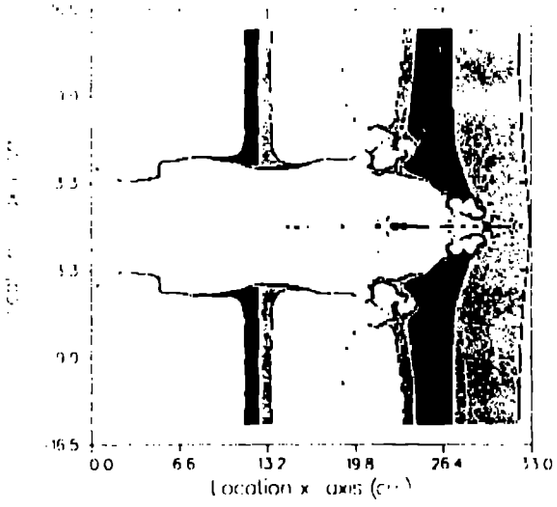

Fig. 5. Deformation of the minimum silica phenolic target.

The maximum pressure P_1 occurred 20 μs after projectile impact. The maximum pressure P_2 occurred after 27 μs. The delay in timing was caused by the time required for the shock wave to travel through the aluminum and polyurethane foam layers of Section 2. The maximum P_1 was 0.73 Mbar and the maximum P_2 was 0.032 Mbar. The large difference was caused by the attenuation of the shock wave by the polyurethane foam. The pressure integral value calculated for this target at Location 1 was 0.56 Mbar•μs and the $P^2\tau$ value at Location 2 was 1.8×10^{-3} Mbar^2•μs.

Target with Minimum Silica Phenolic Thickness

The first target characteristic investigated in the study was the silica phenolic layer. The results of the computation for the projectile impact with the target that had the minimum thickness of silica phenolic (1.0 cm) are shown in Fig. 5. Figure 5 shows the material deformation of the target after 100 μs, when the rates of deformation of Section 1 were small. The projectile produced a hole 9 cm in diameter in this section of the target. In marked contrast, the crater in Section 2 was still growing. The spike in the crater's center was low in density and did not persist to later times.

The P_1 reached a maximum of 1.3 Mbar after 15 μs, and the P_2 reached a maximum of 0.077 Mbar after 21 μs. The pressure integral at Location 1 was 1.2 Mbar•μs and the $P^2\tau$ value at Location 2 was 9.6×10^{-3} Mbar^2•μs. The maximum pressures, pressure integral, and $P^2\tau$ value were significantly increased from those for the nominal target. The time required to develop maximum pressures was reduced in comparison with that of the nominal target.

Target with Maximum Silica Phenolic Thickness

Figure 6 shows the results obtained for the projectile impact with the target that had the maximum silica phenolic thickness (3.0 cm). Deformation of the target 100 μs after impact by the projectile is shown in Fig. 6. The resultant hole in Section 1 was 12 cm in diameter. The deformation of the back of the target on the centerline is similar to that for the nominal target (Fig. 2) and less than that for the minimum silica phenolic thickness target (Fig. 5). The P_1 reached a maximum of 0.30 Mbar after 22 μs and the P_2 reached a maximum of 0.084 Mbar after 32 μs. The pressure maxima occurred at later times than for the nominal target. The pressure integral value at Location 1 was calculated to be 0.56 Mbar•μs, and the $P^2\tau$ value at Location 2 was [illegible] Mbar^2•μs.

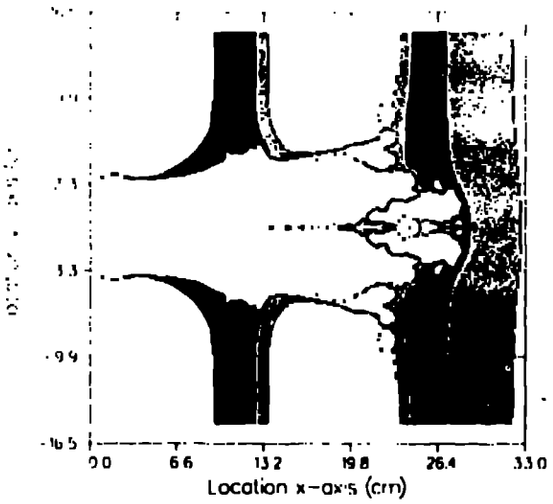

Fig. 6. Deformation of the maximum silica phenolic target.

Target with Minimum Aluminum Thickness

The next target characteristic to be varied was the aluminum layer adjoining the silica phenolic. At 100 μs after projectile impact with the target that had the minimum aluminum thickness (0.2 cm), the target was deformed, as shown in Fig. 7. The diameter of the hole produced by projectile perforation of Section 1 was 10 cm.

The maximum pressure of 1.0 Mbar at Location 1 occurred after 17 μs. The pressure integral value calculated at this location was 0.93 Mbar•μs. The maximum pressure of 0.062 Mbar at Location 2 was found to occur after 23 μs. From the pressure-vs-time curve a $P^2\tau$ value of 7.5×10^{-3} $Mbar^2$•μs was determined. The peak pressure at Location 1 occurred slightly sooner and was slightly higher than that for the nominal target. The maximum pressure at Location 2 also occurred sooner than that for the nominal target and the pressure was also higher.

Target with Maximum Aluminum Thickness

When the aluminum layer adjoining the silica phenolic was set to its maximum value of 2.0 cm, the results shown in Fig. 8 were obtained. Figure 8 shows the target deformation after 100 μs. At this time, the Section 1 hole diameter was 12 cm. Target deformation was considerably less than that for the minimum aluminum target (Fig. 7).

The maximum pressure at Location 1 was found to be 0.33 Mbar 27 μs after projectile impact. The corresponding pressure integral value was calculated to be 0.28 Mbar•μs. The pressure at Location 2 reached a maximum of 0.013 Mbar after 37 μs. The $P^2\tau$ value at this location was 0.24×10^{-3} $Mbar^2$•μs

Target with Minimum Void Extent

The third target characteristic investigated was the extent of the void region between Sections 1 and 2. The results obtained when the void region was at its smallest (1.0 cm) are shown in Fig. 9. In Fig. 9, the target deformation is shown after 100 μs. The hole diameter in Section 1 was 11 cm.

The pressure at Location 1 reached a maximum of 0.68 Mbar after only 7 μs. The pressure integral value was 1.3 Mbar•μs. At 12 μs after projectile impact, the pressure at Location 2 reached a maximum of 0.079 Mbar. The $P^2\tau$ value at this point was calculated to be 5.1×10^{-3} $Mbar^2$•μs.

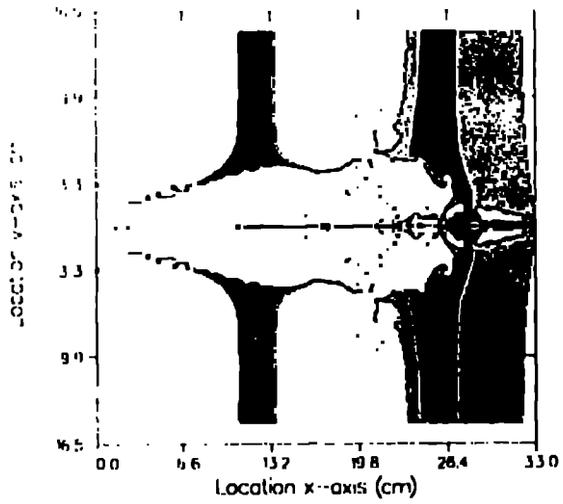

Fig. 7. Deformation of the minimum aluminum target.

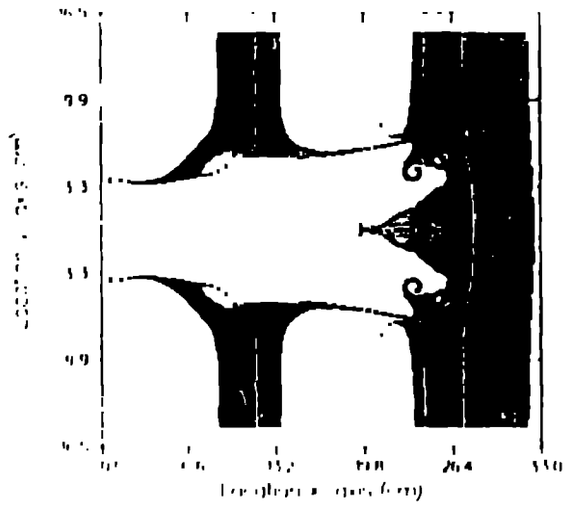

Fig. 8. Deformation of the maximum aluminum target.

The maximum pressure at Location 1 was approximately the same as that for the nominal target but it occurred much sooner. The maximum pressure at Location 2 also occurred much sooner than that for the nominal target, but its value was significantly larger than that for the nominal target.

Target with Maximum Void Extent

When the target included the maximum void region of 18 cm, the results shown in Fig. 10 were obtained. The pressure at Location 1 reached a maximum of 0.50 Mbar after 37 μs, while that at Location 2 reached a maximum of 0.022 Mbar after 41 μs. The calculated pressure-time integral value at Location 1 was 0.32 Mbar-μs. The P^2 value at Location 2 was 1.0×10^{-4} Mbar^2-μs. The crater hole diameter after 100 μs was 12 cm.

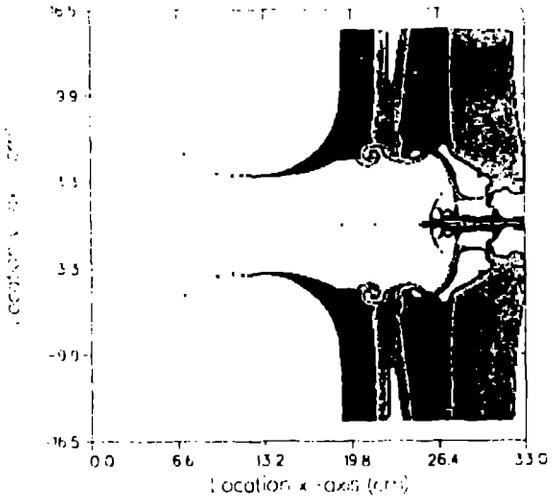

Fig. 9. Deformation of the minimum void target.

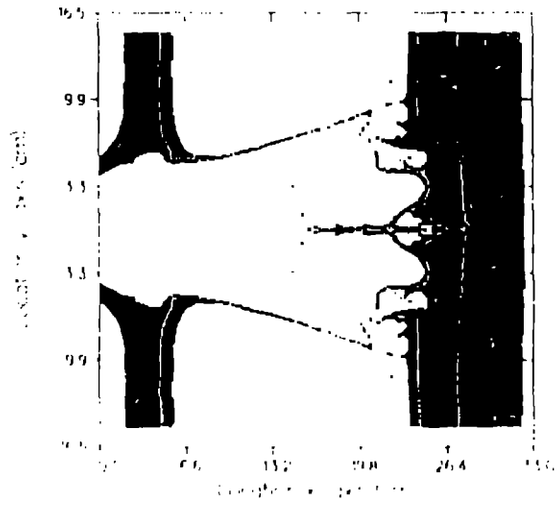

Fig. 10. Deformation of the maximum void target.

Target deformation was much less than that for the minimum void target (Fig. 9). The projectile and Section 1 debris were spread much more in the transverse direction in the maximum void target as compared with those in the minimum void or nominal targets.

Target with Minimum Polyurethane Foam Thickness

The final target characteristic to be varied was the thickness of the polyurethane foam layer between the two fixed layers of aluminum in the back section of the target. The minimum thickness of this layer was zero, that is, there was no polyurethane foam. In this case Section 2 of the target consisted of 6.0 cm of aluminum, with only 1 cm separating Locations 1 and 2 on the centerline. The target deformation 100 μs after projectile impact is shown in Fig. 11. The diameter of the hole in Section 1 was 12 cm.

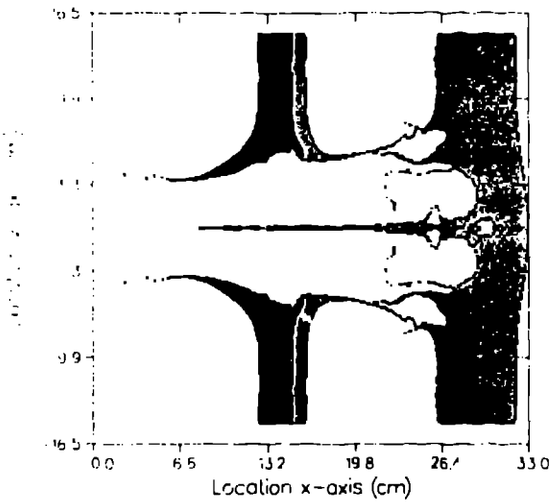

Fig. 11. Deformation of the minimum polyurethane foam target.

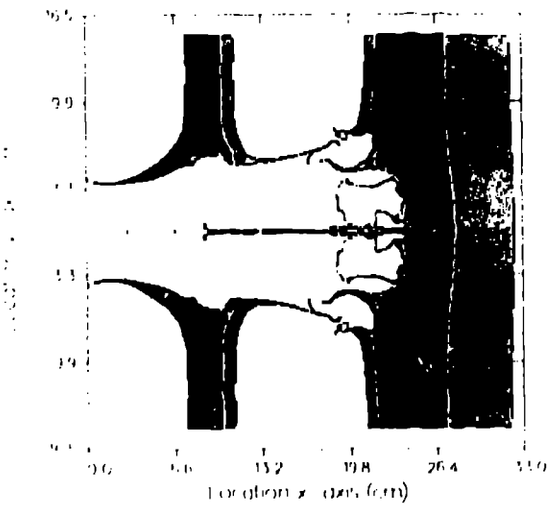

Fig. 12. Deformation of the maximum polyurethane foam target.

The maximum pressure at Location 1 was 0.73 Mbar, and it occurred after 20 μs, while that at Location 2 was 0.079 Mbar and occurred after 25 μs. The pressure integral at Location 1 was 0.56 Mbar•μs and the P^2t value at Location 2 was 4.9×10^{-3} $Mbar^2$•μs. The maximum pressures are much closer together in time than they are for the other targets because of the absence of any intervening foam layer.

Target with Maximum Polyurethane Foam Thickness

The maximum polyurethane foam thickness considered in this investigation was 5 cm. The results for this target are shown in Fig. 12, where the target deformation 100 μs after projectile impact is shown. At this time the hole diameter in Section 1 was 1.2 cm.

The pressure at Location 1 reached a maximum of 0.73 Mbar after 20 μs. The pressure integral value was 0.56 Mbar•μs. The pressure at Location 2 reached a maximum of 0.012 Mbar at 37 μs after projectile impact. The resultant $P^2\tau$ value was found to be 0.29×10^{-3} Mbar^2•μs. The pressure at Location 2 was much lower and arrived much later than that at Location 1, because of the large amount of polyurethane foam (with low shock speed) between the layers.

SUMMARY AND CONCLUSIONS

The hole sizes produced in Section 1 of the target by the projectile impact are given in Table 2 for the four cases in which the target characteristic affected the hole size. The void region and the polyurethane foam layer were found, as expected, to have no effect on the Section 1 hole size. These hole sizes were the same as for the nominal target. The hole sizes listed can be compared with the 12-cm hole size produced in the nominal target. The hole size increased as the silica phenolic or aluminum layers were increased and was relatively independent of the type of material used.

These results are in good agreement with holes produced experimentally in shields (Gehring 1970). In both studies the hole size was found to be fairly independent of shield material and to increase with shield thickness. The hole diameters in Table 2 are within 1 cm of the experimental results reported by Gehring. The trend of the results is also in agreement with numerical analyses of thin-layered targets (Oyer 1986). As the targets become thinner, the hole sizes produced by the projectile decrease and approach the diameter of the projectile for very thin targets.

Table 2. Hole diameter in section 1 (cm)

Target Component	Component Thickness		
	Minimum	Nominal	Maximum
Silica phenolic	9	12	12
Aluminum	10	12	12

Comparison of Figs. 5 through 8 shows that the spread of projectile and Section 1 debris increased as the silica phenolic or aluminum layers were increased in thickness. These results are also in agreement with experimental results (Gehring 1970).

The maximum pressures at Location 1 of the target are summarized in Table 3 for all four target characteristics considered. These values can be compared with the maximum pressure of 0.73 Mbar found at this location in the nominal target. In all cases except one, the maximum pressure at Location 1 was substantially less for the maximum thickness than it was for the minimum thickness target. The exception was observed for the polyurethane foam layer, where the maximum pressures were equal for minimum and maximum layer thicknesses. This result is reasonable because the polyurethane foam layer was behind Location 1, and changes in this layer would not affect the pressures ahead of it.

Table 3. Maximum pressure at location 1 (Mbar)

Target Component	Component Thickness		
	Minimum	Nominal	Maximum
Silica phenolic	1.3	0.73	0.30
Aluminum	1.0	0.73	0.33
Void	0.68	0.73	0.50
Polyurethane	0.73	0.73	0.73

The arrival times of the maximum pressures at Location 2 are shown in Table 4 for all four target characteristics considered. The time of occurrence of this pressure for the nominal target was 27 μs. The time to achieve maximum pressure in the nominal target was intermediate to that for the minimum and maximum layer thicknesses in all cases. Greater thicknesses of the target component were found to delay development of the maximum pressure in all cases. Variations in the void extent were found to have the greatest effect on the arrival time of the maximum pressure at Location 2 because of the time required for the debris from the projectile, silica phenolic, and aluminum to traverse the void region.

Table 4. Time to develop maximum pressure at location 2 (μs)

Target Component	Component Thickness Minimum	Nominal	Maximum
Silica phenolic	21	27	32
Aluminum	23	27	37
Void	12	27	41
Polyurethane	25	27	37

The time integrated pressures at Location 1 are summarized in Table 5 for all of the target characteristics that were varied in the study. The values for the maximum layer thickness were less than those for the minimum layer thickness for all target characteristics except polyurethane foam. Since the polyurethane foam layer is behind Location 1, variations in this layer were not expected to change the pressure integral conditions from that for the nominal target. The pressure integral value for the nominal target was 0.56 Mbar•μs. This value was intermediate to the values for the minimum and maximum thicknesses of aluminum and void regions. The pressure integral value obtained for the maximum silica phenolic target was the same as that for the nominal target.

Table 5. $\int$ Pdt at location 1 (Mbar•μs)

Target Component	Component Thickness Minimum	Nominal	Maximum
Silica phenolic	1.2	0.56	0.56
Aluminum	0.93	0.56	0.28
Void	1.3	0.56	0.32
Polyurethane	0.56	0.56	0.56

The lower values of pressure and pressure integral for greater thicknesses of silica phenolic and aluminum were caused by increased erosion of the projectile and increased dispersion of the debris from the perforation of Section 1. The lower values for greater void extent were caused by increased transverse dispersion of the projectile and Section 1 debris, because it had a longer time to disperse before striking Section 2 of the target.

The $P^2\tau$ values at Location 2 are summarized in Table 6 for the four varied target characteristics. The $P^2\tau$ value found at this location for the nominal target was 1.8×10^{-3} Mbar^2•μs. In all cases the $P^2\tau$ values for the maximum thicknesses were less than those for the minimum thicknesses, and the $P^2\tau$ value for the nominal target was intermediate to the values for the extremes. This trend agrees with the expected trend. As the thicknesses of the silica phenolic and aluminum layers are increased to the point at which the projectile will no longer perforate these layers, the $P^2\tau$ value must go to zero. Similarly, as the void extent is increased, the debris cloud becomes more diffuse, and the centerline pressure on Section 2 decreases. Also, as the polyurethane foam thickness increases, the shock becomes more attenuated, and the $P^2\tau$ value approaches zero.

Table 6. $P^2\tau$ at location 2 (10^{-3} Mbar^2•μs)

Target Component	Component Thickness Minimum	Nominal	Maximum
Silica phenolic	9.6	1.8	0.86
Aluminum	7.5	1.8	0.24
Void	5.[illegible]	1.8	1.0
Polyurethane	4.9	1.8	0.29

The $P^2\tau$ values at Location 2 are plotted in Fig. 13 as functions of layer thicknesses for all of the target characteristics that were varied. The percentage rate of decrease of $P^2\tau$ value is greater for larger layer thicknesses for all of the target characteristics except the void region. For the void region, the percentage rate of change of $P^2\tau$ value is approximately constant.

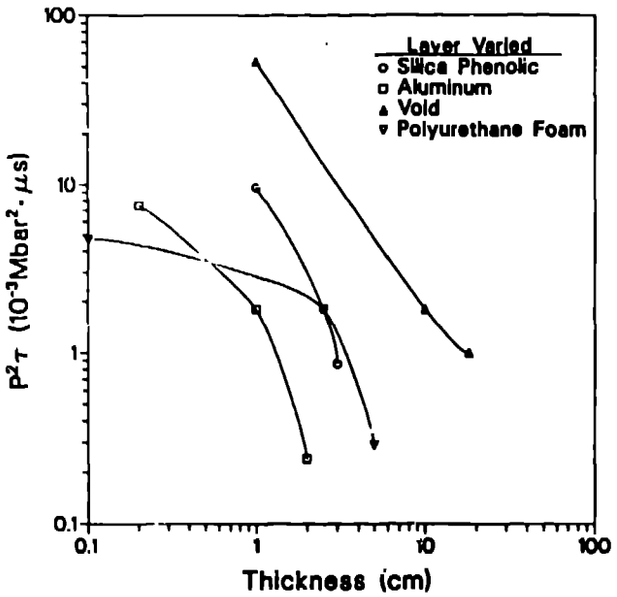

Fig. 13. $P^2\tau$ value at Location 2 as a function of layer thicknesses.

An aluminum layer of the same thickness as silica phenolic produced a lower $P^2\tau$ value. This relationship was caused by the higher density of aluminum. An equal thickness of silica phenolic has a lower areal mass, which is the product of material density and layer thickness, than aluminum and erodes the projectile less as it perforates the Section 1 layers. The consequence was a higher pressure produced in Section 2 of a target with a given thickness of silica phenolic as compared with a target with an equal thickness of aluminum. However, on a per unit mass basis, increasing the silica phenolic thickness is slightly more effective in reducing the $P^2\tau$ value than is aluminum.

Changes in polyurethane foam thickness produced a relatively smaller change in $P^2\tau$ values as compared with changes in the silica phenolic and aluminum layers. The $P^2\tau$ value approached 4.9×10^{-3} Mbar^2•μs as the polyurethane foam thickness went to zero. For larger values of polyurethane foam thickness, however, the rate of change of $P^2\tau$ value approached that for silica phenolic and aluminum.

The results shown in Fig. 13 can be used to determine the $P^2\tau$ value expected for a target, other than those previously analyzed, by assuming that each of the target components independently affects the $P^2\tau$ value. Figure 13 was used to predict a $P^2\tau$ value of 6.8×10^{-3} Mbar^2•μs for a target with 2.0 cm of silica phenolic, 0.5 cm of aluminim, a 5.0-cm void, and 4.0 cm polyurethane foam. A PINON computation of this case resulted in a $P^2\tau$ value of 6.9×10^{-3} Mbar^2•μs, which is in very good agreement with the predicted value. In this way, the $P^2\tau$ value for a myriad of complex targets can be calculated without detailed numerical simulations of each target.

ACKNOWLEDGEMENT

The author would like to acknowledge the assistance of P. A. Pope in conducting this study and for writing the computer programs that improved the postprocessing capabilities and led to the results presented here.

This study was funded by the United States Department of Energy.

REFERENCES

Boettger, J. C. (March 1989). SESAME equation of state for a polymer composite: phenolic refrasil. Los Alamos National Laboratory report LA-11512-MS.

Gehring, J. W. (1970). Theory of impact on thin targets and shields and correlation with experiment. In: High Velocity Impact Phenomena (R. Kinslow, Ed.), Academic Press, New York and London.

Holian, K. S. (November 1984). T-4 handbook of material properties data bases. Los Alamos National Laboratory report LA-10160-MS.

Johnson, W. E. and Anderson, Jr., C. E. (1987). History and application of hydrocodes in hypervelocity impact. In: International Journal of Impact Engineering, Vol. 5, No. 1-4 (Pergamon Press, New York) 423-439.

Meier, R. W. (1987). Numerical simulations of small projectiles impacting a multilayered target at hypervelocities. In: International Journal of Impact Engineering, Vol. 5, No. 1-4 (Pergamon Press, New York) 471-481.

Oyer, A. T. (1986). Bumper shield analysis. Los Alamos National Laboratory report LA-10788-MS.

Walker, F. E. (1976). Discussion on shock initiation and $P^2\tau$. In: Proceedings of the Sixth International Symposium on Detonation, August 24-27, 82-85.

Walker, F. E. and Wasley, R. J. (1969). Critical energy for shock initiation of heterogeneous explosives. UCRL-70891, Explosivstoffe, Vol. 17, No. 1, 9.

Youngs, D. L. (1982). Time-dependent multimaterial flow with large fluid distortion. In: Numerical Methods for Fluid Dynamics, (K. W. Morton and M. J. Baines, Eds., Academic Press, New York and London).